Appendix I

Kappa Analysis

ESTIMATION OF KAPPA

Final Report, Rev 1
2/18/2014
Pacific Engineering and Analysis
Prepared by
Walter Silva
Bob Darragh

Prepared for:
Pacific Northwest National Laboratory
902 Battelle Boulevard
Richland, WA

TABLE OF CONTENTS

TABLES

Figures

1.0 ESTIMATION OF KAPPA

For typical rock and deep soil sites which display an overall increase in stiffness with depth due primarily to increasing confining pressure, the major contribution to energy dissipation at a site occurs over the top 1 to 2 km of the crust (Anderson and Hough, 1984; Silva and Darragh, 1990). This observation was first recognized and subsequently characterized as a site parameter by Anderson and Hough (1984), specifically as kappa at zero epicentral distance. Due to geologic processes sites which reflect significant departures from an overall increase in stiffness with depth, such as layered basalt and sedimentary soil or rock sequences, significant contributions to kappa may occur at depths well beyond 1 to 2 km and reflect contributions from both intrinsic energy dissipation as well as scattering. This damping appears to be frequency-independent (hysteretic), occurs at low strains, and is the principal site or path parameter controlling the limitation of high-frequency (> 5 Hz) strong ground motion at close in (≤ 50 km) sites. As a result, its value or range of values is important in characterizing strong ground motions for engineering design, particularly in regions of sparse seismicity. Additionally, because it is generally independent of the level of motion at rock or very stiff sites, small local or regional earthquakes may be used to estimate its value or range in values. For the Hanford site area, which has shallow soil overlying layered basalts likely resting on several kilometers of sediments over crystalline basement, estimation of the damping in the basalt sequence is important to assessing appropriate levels of high-frequency design motions.

For the facilities located at the Hanford site, kappa estimates for both the Saddle Mountain basalts (SMB) as well as the underlying Wanapum basalts (WB) are desired to characterize design motions. To provide recordings sampling both crustal structures, windowed shear-wave Fourier amplitude spectra (FAS) and pre-event noise samples were provided for

SMB sites HAWA, E07A, E08A, F07A and WB sites D08A and E09A. In total the data set included 59 earthquakes recorded in the 2005 to 2013 time frame (Al Rohay personal communication, 08/27/2013). With the exception of two recordings at HAWA, which has both broadband velocity and accelerograph instruments, all the other sites have only broadband velocity instruments (US Array or Transportable array (TA)) with sampling at 40 SPS and a corresponding high-frequency limit of 18 Hz. The accelerograph recordings have a sampling rate of 200 SPS with a high-frequency limit of 80 Hz. The narrow bandwidth for the broadband data, particularly at 15 Hz for 2004 analysis, severely limits resolving power for kappa resulting in some ambiguity in kappa at site HAWA between the 2004 (PNNL, 2005) and the current analyses.

To provide an analysis data subset based on a comparison of signal verses noise levels, use of only deep ($\geq$ 5 km) hypocenters to fully sample the supra WB sediments and avoid possible double paths in the sediments for downgoing paths at distant sites, maximize the number of sites with common earthquakes, and provide consistency with the earlier 2004 (deep and far) analyses, a subset of 15 earthquakes was selected from the 2005 to 2013 data set. The final analysis data set consists of the 15 2005 to 2013 earthquakes in addition to the 10 recordings at HAWA from the 2004 (PNNL, 2005) data set. Table 1 lists the two data sets, magnitudes, hypocentral depths and distances, as well as the distributions between the six recording stations. Tables 2 and 3 reflect more detailed catalogues for the 2004 kappa analysis (PNNL, 2005) and more recent recordings respectively.

An inversion process was used to estimate kappa in which the earthquake source, path, and site parameters were obtained by using a nonlinear least-squares fit to the Fourier amplitude spectra (FAS) using the point-source model (Boore 1983; EPRI 1993). The useable bandwidth

for each amplitude spectrum was site and earthquake specific based on a visual examination of the pre-event FAS noise levels compared to the windowed shear-wave FAS and with the maximum frequency constrained by filters, 15 Hz for 2004 data and 18 Hz for the 2005 to 2013 data. Typically the inversion bandwidth is magnitude dependent extending to lower frequency as magnitude increases and averaged around 0.5 Hz for $\mathbf{M} \geq 2$ and around 1.0 Hz below $\mathbf{M} \approx 2$. The inversion scheme treats multiple earthquakes and sites simultaneously with the common crustal path damping parameter Q(f). The parameter covariance matrix was examined to determine which parameters may be resolved for each data set. Asymptotic standard errors were computed at the final iteration. The five parameters that may be determined from the data are kappa (site-specific attenuation), Q_0 (the value of Q for f equal to 1 Hz), and η (frequency-dependent path Q model), **M**, and corner frequency (stress drop). The procedure uses the Levenberg-Marquardt algorithm (Press et al. 1986) with the inclusion of the second derivative. Crustal profile amplification was accommodated in the inversion scheme by incorporating the appropriate transfer functions (source depth to surface) in estimating the point-source surface spectra.

To reduce the potential for non-uniqueness inherent in inversion results, a suite of starting models was employed. The final set of parameters was selected based upon a visual inspection of the model fit to the Fourier amplitude spectrum, the chi-square values, and the parameter covariance matrix.

The stress drop was calculated from the moment and corner frequency using the relation

$$f_c = \beta \left(\frac{\Delta \sigma}{8.44 \cdot M_o} \right)^{\frac{1}{3}} \quad (1)$$

The inversions were done on log amplitude spectra (vector average (SRSS) of the two horizontal components), as strong ground motion data appear to be log normally distributed. This is consistent with the model being represented as a product (rather than sum) of models (EPRI 1993). A feature of the inversion scheme is the flexibility to distinguish between sites, for which kappa is determined, and stations for which recordings are available. As a result several stations may share a common site or kappa estimate. This feature permitted grouping separately Saddle Mountain and Wanapum analogs as well as provide insights into apparent differences in kappa at station HAWA between the 2004 analysis (PNNL, 2005) and the current analysis reflecting the additional 2005 to 2013 recordings.

For the inversions, due to the narrow bandwidth and distance limitation with few recordings beyond 100 km, Q(f) was fixed at $500(f)^{0.6}$. The assumed Q(f) exceeds that of about 300 $f^{0.4}$ (Phillips et al., 2013; as contained in Adrian Rodriquez-Marek WM3, 2013). The exceedence of the Phillips et al. (2013) Q(f) was to approximately compensate for their exclusion of kappa. The assumed higher Q(f) used in the inversions assumes some portion of their frequency dependent damping would likely be partitioned into frequency independent hysteretic damping (kappa), resulting in higher Q(f). Using the Phillips et al. (2013) Q(f) in the inversions may then bias Hanford kappa to higher and potentially unconservative values.

For the transfer functions, amplification (FAS) from the source (nominally depth of 10 km) to the surface, three crustal models were used:

1) An average regional model with a surface shear-wave velocity of 2,080m/s and 3,430m/s at a depth of 10 km (Al Rohay, personal communication, 10/11/2001). This transfer function was initially applied at all the sites (Table 1).
2) For the unique profile at HAWA, the site-specific profile to crystalline basement

(Julian Bommer personal communication, 9/6/2013) was used to develop amplification from crystalline basement at a shear-wave velocity of 3,500m/s to the surface, concrete floor of the bunker at 1,500m/s. The HAWA profile has numerous velocity inversions resulting in a rapidly oscillating amplification with a highly smoothed illustration shown in Figure 1. An examination of the FAS at HAWA did not reveal the deep and broad dip near 10 Hz but rather stable peaks at around 5 Hz and 13 Hz. As a result the HAWA amplification was not used in favor of the smooth Hanford transfer function with similar overall amplification.

3) Because the two WB sites (D08A, E09A, Table 1) and, unexpectedly SMB site E08A, show significantly higher high-frequency amplification than the other sites, amplification was developed for profile D08A (Julian Bommer, personal communication, 9/15/2013). As Figure 1 illustrates the shallow soil over firm to hard rock has significant amplification beyond about 5 Hz to 8 Hz.

For the initial inversions there was an inconsistency in the kappa value at HAWA between the 2004 (PNNL, 2005) data and analyses and the 2005 to 2013 data and analyses. The earlier results suggested a kappa around 0.02s while separate analyses with the more recent data resulted in a much larger value near 0.06s. Combining the two data sets and separating station HAWA into three sites (three kappa values) HAWA05-13 (more recent data), HAWA04 (2004 recordings), and HAWA BB (two accelerograph recordings of two of the earthquakes in the HAWA 05-13 suite) resulted in consistently high kappa (≈ 0.06s) for the more recent data at both the broadband accelerograph site as well as the HAWA 05-13 site. For HAWA04 however, the kappa estimate remained annoyingly low (about 0.02s). Because the HAWABB results showed both good fits out to 25 Hz, the limit of the useable frequency range, and consistency with the

HAWA05-13 results, credibility was attached to the higher kappa estimates. These preliminary indications suggested an increase in epistemic uncertainty with increasing information, an unusual occurrence. However, closer scrutiny suggested that a possible issue was the subset of five small magnitude (**M** < 2) earthquakes in the 2004 data set (Tables 1 and 2). While the best solution (minimum chi-square) resulted in corner-frequencies below 15 Hz and very low stress drops (< 1 bar), another solution may exist with corner frequencies exceeding 15 Hz and not resolvable with the 15 Hz high-frequency limit. This potential issue was examined by extending the high-frequency limit to 16 Hz for the 2004 data whereupon kappa increased to about 0.05s. To remedy the issue and include as much of the data as possible, the corner frequencies for **M** < 2 were fixed beyond 15 Hz with the high-frequency limit retained at 15 Hz. Note for the point-source model with a corner-frequency beyond 15 Hz, the corner-frequency will have little effect for frequencies below 15 Hz.

To continue with the inversions the four SMB and two WB analog stations were added as sites as reflected in Table 4. For the Case 1 inversions, eight kappa values were estimated with corner frequencies free for the 2004 data and the Hanford (Figure 1) crustal model amplification applied for each site. Note the inversion resulted in low kappa estimates at SMB sites E08A, HAW04, and WB sites D08A, and E09A. For Case 2, corner-frequencies were fixed > 15 Hz for 2004 data with **M** < 2 with an increase in kappa for HAWA04 from 0.022s to 0.058s, now generally consistent with HAWA05-13 recordings as well as HAWABB, the two accelerograph recordings. Additionally the maintenance of the remaining kappa estimates between Cases 1 and 2 is encouraging suggesting little coupling between sites in the inversions.

In the analyses of Cases 1 and 2 as well as many others, it was observed that SMB site E08A and WB sites D08A and E09A consistently showed much larger and similar high-

frequency (≥ 5 Hz) motions and lower kappa estimates than SMB sites HAWA, E07A, and F07A, with much larger kappa estimates. To mitigate the possibility of unconservative low kappa estimates, amplification for WB profile D08A was applied for these three sites resulting in Case 3. As Table 4 shows, Case 3 kappa estimates increased considerably for these three sites and remained reasonably consistent for the remaining sites, suggesting reasonable stability in kappa brought about through the additional recordings subsequent to 2004 and, importantly, the inclusion of the two accelerograph recordings at HAWA. For kappa analyses for **M** < 2, two solutions likely exist, each with associated kappa estimates (populations) and ranges in epistemic uncertainty that may not overlap. As a result it is not sufficient to determine kappa over the constant displacement range, consideration must be given to the acceleration range as well unless additional information actually reduces epistemic uncertainty.

For Hanford, it appears there are resolvable differences in kappa between SMB and WB sites but SMB station E08A shows more of the high-frequency characteristics of WB.

For a visual consideration of the fits Figures 2 through 9 compare model and recording FAS (smoothed) for each of the sites. Figure 2 shows the FAS at HAWA reflecting the 10 earthquakes from the 2004 analyses (PNNL, 2005) with earthquake numbers listed in Table 2. From Figure 2 the dominance and consistency of the resonances at around 5 Hz and around 12 Hz are apparent, suggesting fairly shallow discontinuities in shear-wave velocity. Note a 15 Hz resonance would be the first overtone for a 5 Hz fundamental. Figures 3 and 4 show the FAS at HAWA reflecting the 15 additional earthquakes (Tables 1 and 3). Figure 3 shows results for the TA array recordings while Figure 4 shows accelerograph recordings for the two earthquakes of this subset which were also recorded on the TA array. Both Figures 3 and 4 show the two resonances but with somewhat less dominance and consistency than shown in Figure 2.

For the remaining SMB sites Figures 5, 6, and 7 shows results for sites E07A, E08A, and F07A respectively. From this suite of Figures the difference in character of the FAS beyond a few Hz for site E08A (Figure 6) is readily apparent, suggesting either a very low kappa value or a moderate kappa value coupled with high-frequency amplification, as interpreted in the analyses.

Finally the WB sites are reflected in Figures 8 and 9 for sites D08A and E09A respectively. Both of the WB sites show FAS at high-frequency distinctly apart from SMB sites HAWA (Figures 2, 3, and 4), E07A (Figure 5), and F07A (Figure 7) and similar overall shapes to SMB site E08A (Figure 6). The trends suggest broadly similar kappa values for sites with similar high-frequency shapes, conditional on similar amplification, as assumed in the analyses.

2.0 ASSESSMENT OF UNCERTAINTY IN KAPPA

To examine model (kappa) sensitivity and provide a basis for model uncertainty, fixed parameters were varied by realistic amounts to assess differences in kappa. Model parameters include R_C (cutoff distance from 1/R to $1/\sqrt{R}$ geometrical attenuation), Q_o, eta, $\Delta\sigma$ (bars), Brune point-source shear-wave velocity (β) and density (ρ), **M**, and crustal amplification (f). Inversion parameters typically consist of **M**, Q_o, eta, R_C, and kappa. For data sets with an insufficient range in distances, strong coupling necessitates fixing both Q_o and eta and occasionally R_C, which was the case for Hanford. Initial parameter for the Hanford analyses were as follows:

M = given,

Q_o = 500,

eta = 0.6,

β = 3.5 km/s,

ρ = 2.5 cgs,

R_C = 80 km,

Crustal amplification: Hanford Crustal Model, HAWA, D08A as illustrated in Figure 1. Inversions were done for $\Delta\sigma$ (f_c), **M**, kappa for eight sites (Table 4).

Starting values were:

$\Delta\sigma$ = 5 bars,

Kappa = 0.04s at all eight sites.

Table 5 shows the change in kappa for a given change in each parameter as well as starting models for κ and $\Delta\sigma$. Note all inversion parameters (**M**, $\Delta\sigma$) change along with kappa. From Table 5 the strongest coupling was with η with a 40% reduction in median kappa for a 50% reduction in η. Recall our kappa estimates must be viewed as relative to Q(f) and R_C, which suggests an uncertainty in median (over the eight sites) kappa of about 0.4, for a realistic range in parameters, taken independently.

As an additional approach to estimate epistemic uncertainty in kappa, inversions with different subsets of the data (jackknife) were considered. However, upon consideration, there were insufficient data to meaningfully constrain the inversions. Some inference along these lines may be gained from Table 4. The table compares HAWA05-13, and HAWA04 earthquakes recorded at station HAWA inverted for different site kappas. With the 2004 corner frequencies for **M** < 2 fixed > 15 Hz, the two kappa estimates differ by about 5%. Summarily the two truly broadband recordings, HAWABB in Table 4 at station HAWA, included in the 2005-2013 suite of earthquakes analyzed, also show a similar site kappa, differing with HAWA04 by about 4%.

Additional insight into kappa uncertainty is the effect of smoothing. Typically inversions are done on unsmoothed spectra when the useable bandwidth is quite limited. This avoids the loss of smoothing (degrees of freedom) for wide smoothing windows as the ends of the band are

approached. Also unsmoothed FAS results in a naturally higher weight at high frequency (more points) where we desire the emphasis for kappa inversions and there is less interest in **M**. For log frequency increment smoothing, smoothed FAS are at equal spacing in log frequency giving equal weigh across the inversion bandwidth. We also added this to the sensitivity analysis with a difference in median kappa between unsmoothed and smoothed (log frequency increment = 0.1) FAS inversions of about 1.02 or 2%.

Epistemic uncertainty in kappa, due largely to the sensitivity with η in this data set, around a value of 0.4 seems warranted, with the assumption the change in median kappa over the eight sites may be taken for an individual site. With cross correlations between site kappa values of about 0.8, a maximum individual site uncertainty of about 0.4 may be reasonable for a median kappa uncertainty of 0.4.

3.0 STRESS DROPS

To assess stress drops, of the subset of 25 earthquakes (10 from the 2004 analyses; PNNL, 2005) a total of 14 were judged to have resolvable corner frequencies with potentially meaningful stress drops. It is important to note the magnitudes changed from the catalog values by significant amounts ($\approx$ 0.5 unit) in some cases (PNNL, 2005). For the 14 resolvable stress drops, the median estimate was 19.745 bars (fitting on log FAS) with a σ_{ln} of 1.384. The simple $\sigma_{\mu ln}$ was about 0.4. For forward computations incorporating RVT the stress drops should be increased by the mean/median ratio (1.27) from the fit to compensate for fitting log (FAS).

References

Anderson, J. G. and S. E. Hough (1984). "A model for the shape of the Fourier amplitude spectrum of acceleration at high frequencies." *Bull. Seism. Soc. Am.*, 74(5), 1969-1993.

Boore, D.M. (1983). "Stochastic simulation of high-frequency ground motions based on seismological models of the radiated spectra." *Bull. Seism. Soc. Am.*, 73(6), 1865-1894.

Electric Power Research Institute (1993). "Guidelines for determining design basis ground motions." Palo Alto, Calif: Electric Power Research Institute, vol. 1-5, EPRI TR-102293.

Phillips, W.S, K. M. Mayeda, and L. Malagnini (2013). "How to invert multi-band, regional phase amplitudes for 2-D attenuation and source parameters: tests using the USArray." Pure and Applied Geophys. Published online August 8, 2013. DOI 10.1007/s00024-013-0646-1

Pacific Northwest National Laboratory (2005). "*Site-specific seismic site response model for the Waste Treatment Plant, Hanford, Washington*." PNNL-15089. Prepared for the U.S. Department of Energy Office of River Protection under Contract DE-AC05-76RL01830.

Press, W.H., Flannery, B.P., Teukolsky, S.A., Vetterling, W.T. (1986). "Numerical Recipes." Cambridge Univ. Press, Cambridge.

Silva, W.J., and Darragh, R.B. (1990). Engineering Characterization of Strong Ground Motion Recorded at Rock Sites. Electric Power Res. Inst. Draft Report, EPRI RP-2556-48.

Table 1

Earthquake Summary

Station Name	N	M – M	Range Hypo Dist (km)	Range Hypo Depth (km)	Analogy To
HAWA 2004*	10	1.49-3.25	36 - 86	8.7 - 22.1	SMB
HAWA 2013	15	2.4-3.4	32 - 149	5.7 - 21.9	SMB
E07A 2013	10	2.4-3.4	39 - 138	6.4 - 21.9	SMB
E08A 2013	12	2.4-3.4	25 - 140	6.4 - 21.9	SMB
F07A 2013	9	2.4-3.4	46 - 118	6.4 - 21.9	SMB
D08A 2013	8	2.4-3.4	48 - 152	6.4 - 18.0	WB
E09A 2013	10	2.4-3.4	56 - 170	9.2 - 21.9	WB

*Earthquakes analyzed in 2004 (PNNL, 2005)

Table 2

2004 Analysis Catalog (PNNL, 2005)

Station	Magnitude	Hypocentral Distance (km)	Depth (km)	Year, Day	Hr	Min	Sec	Com*	EQ
HAWA	1.49	44.99887	10.89	1999 266	2	24	53.790	N	1
HAWA	3.25	45.83549	12.38	1999 262	11	11	52.919	N	2
HAWA	2.55	86.37135	13.48	2001 114	13	21	29.899	N	3
HAWA	1.51	43.56913	13.19	2001 154	11	51	58.540	N	4
HAWA	2.63	66.48337	20.08	2001 158	12	45	42.639	N	5
HAWA	3.17	80.96331	11.04	2003 15	3	41	58.400	E	6
HAWA	3.17	80.96331	11.04	2003 15	3	41	58.400	N	
HAWA	1.63	44.67281	17.79	2003 35	16	33	39.580	N	7
HAWA	1.63	44.67281	17.79	2003 35	16	33	39.580	E	
HAWA	2.63	68.85155	8.78	2003 54	7	54	.140	E	8
HAWA	2.63	68.85155	8.78	2003 54	7	54	.140	N	
HAWA	1.81	42.15794	22.10	2003 134	4	59	43.770	E	9
HAWA	1.81	42.15794	22.10	2003 134	4	59	43.770	N	
HAWA	1.58	35.80111	8.72	2004 230	19	44	51.400	E	10
HAWA	1.58	35.80111	8.72	2004 230	19	44	51.400	N	

*Single horizontal component available

Table 3

Catalog of Additional Sites and Earthquakes

Station	Mag	Hypocentral Dist (km)	Hypocentral Depth (km)	Year	Day	Hr	Min	Sec	Eq
HAWA	2.5	42.44886	10.5	2005	314	12	45	59.350	1
HAWA	3.4	86.38833	13.6	2006	354	9	43	26.574	2
E07A	3.4	116.25550	13.6	2006	354	9	43	26.575	2
E08A	3.4	62.42395	13.6	2006	354	9	43	26.574	2
F07A	3.4	112.65720	13.6	2006	354	9	43	26.575	2
D08A	3.4	112.27650	13.6	2006	354	9	43	26.574	2
E09A	3.4	56.16646	13.6	2006	354	9	43	26.574	2
HAWA	3.0	102.14160	5.7	2006	234	1	6	9.598	3
HAWA	3.1	148.61780	6.7	2006	206	6	13	37.375	4
HAWA	2.7	39.35289	21.9	2008	34	23	36	4.350	7
E07A	2.7	56.54786	21.9	2008	34	23	36	4.350	7
E08A	2.7	24.57609	21.9	2008	34	23	36	4.349	7
F07A	2.7	95.83476	21.9	2008	34	23	36	4.349	7
E09A	2.7	82.06871	21.9	2008	34	23	36	4.350	7
HAWA	3.3	31.83565	18.0	2008	139	22	19	54.700	8
E07A	3.3	54.37752	18.0	2008	139	22	19	54.700	8
E08A	3.3	54.84989	18.0	2008	139	22	19	54.700	8
F07A	3.3	46.12018	18.0	2008	139	22	19	54.700	8
D08A	3.3	111.87180	18.0	2008	139	22	19	54.700	8
E09A	3.3	115.01170	18.0	2008	139	22	19	54.700	8
HAWA	3.2	104.05030	9.2	2010	84	22	31	7.149	11
E08A	3.2	96.48579	9.2	2010	84	22	31	7.149	11
D08A	3.2	48.14118	9.2	2010	84	22	31	7.150	11
E09A	3.2	131.95500	9.2	2010	84	22	31	7.150	11
HAWA	2.6	54.53100	12.7	2010	128	19	42	29.900	14
E07A	2.6	38.97710	12.7	2010	128	19	42	29.899	14
E08A	2.6	91.47976	12.7	2010	128	19	42	29.900	14
E09A	2.6	160.94030	12.7	2010	128	19	42	29.900	14
HAWA	2.7	106.76700	20.2	2010	135	16	6	13.275	15
E07A	2.7	137.06190	20.2	2010	135	16	6	13.275	15
E08A	2.7	94.03613	20.2	2010	135	16	6	13.275	15
F07A	2.7	110.51660	20.2	2010	135	16	6	13.275	15
E09A	2.7	93.01365	20.2	2010	135	16	6	13.275	15
HAWA	2.8	108.10540	20.8	2010	136	2	15	17.250	16
E07A	2.8	138.36000	20.8	2010	136	2	15	17.249	16
E08A	2.8	95.63689	20.8	2010	136	2	15	17.250	16
F07A	2.8	111.11040	20.8	2010	136	2	15	17.250	16
E09A	2.8	94.49943	20.8	2010	136	2	15	17.249	16

Table 3 (cont.)

Catalog of Additional Sites and Earthquakes

Station	Mag	Hypocentral Dist (km)	Depth (km)	Year	Day	Hr	Min	Sec	Eq
HAWA	3.2	74.53619	11.0	2012	101	4	43	35.300	28
E08A	3.2	56.59765	11.0	2012	101	4	43	35.300	28
F07A	3.2	96.56850	11.0	2012	101	4	43	35.299	28
D08A	3.2	113.22140	11.0	2012	101	4	43	35.300	28
E09A	3.2	68.07073	11.0	2012	101	4	43	35.300	28
HAWA	3.3	112.78290	12.7	2012	257	17	33	45.300	29
E07A	3.3	89.18053	12.7	2012	257	17	33	45.300	29
E08A	3.3	120.24280	12.7	2012	257	17	33	45.300	29
D08A	3.3	89.68194	12.7	2012	257	17	33	45.300	29
E09A	3.3	170.12950	12.7	2012	257	17	33	45.300	29
HAWA	2.4	54.54874	15.9	2009	80	10	11	37.649	37
E07A	2.4	45.27405	15.9	2009	80	10	11	37.650	37
E08A	2.4	56.44445	15.9	2009	80	10	11	37.649	37
F07A	2.4	113.09280	15.9	2009	80	10	11	37.650	37
D08A	2.4	52.87224	15.9	2009	80	10	11	37.650	37
E09A	2.4	113.06890	15.9	2009	80	10	11	37.650	37
HAWA	2.8	92.44021	7.7	2009	149	18	54	4.400	55
E07A	2.8	123.20480	7.7	2009	149	18	54	4.400	55
E08A	2.8	75.16523	7.7	2009	149	18	54	4.400	55
F07A	2.8	106.67030	7.7	2009	149	18	54	4.400	55
D08A	2.8	130.13790	7.7	2009	149	18	54	4.400	55
HAWA	2.5	108.26800	6.4	2009	157	13	22	11.750	56
E07A	2.5	79.09200	6.4	2009	157	13	22	11.750	56
E08A	2.5	140.12330	6.4	2009	157	13	22	11.750	56
F07A	2.5	117.51150	6.4	2009	157	13	22	11.750	56
D08A	2.5	151.64390	6.4	2009	157	13	22	11.750	56

Table 4 Hanford Kappa Evaluation				
		2004, 2005 to 2013 Data κ(s)		
Site		Case 1	Case 2	Case 3
1	HAWA05-13	0.061	0.061	0.064
2	E07A	0.068	0.068	0.072
3	E08A	0.010	0.010	0.034
4	F07A	0.056	0.056	0.061
5	HAWA04	0.022	0.058	0.058
6	D08A	0.015	0.015	0.039
7	E09A	0.	0.	0.016
8	HAWABB	0.056	0.056	0.058

Case 1: Hanford (Figure 1) amplification at all sites,
Case 2: Hanford (Figure 1) amplification at all sites, 2004 earthquakes **M** < 2 f_c fixed > 15 Hz,
Case 3: WANAPUM (D08A) amplification at E08A, D08A, E09A; HAWA amplification at remaining sites, 2004 earthquakes **M** < 2 f_c fixed > 15 Hz.

	2004 Data κ(s)	
Site	Case 1	Case 2
HAWA	0.022	0.058

Case 1: HAWA amplification,
Case 2: HAWA amplification, 2004 earthquakes **M** < 2 f_c fixed > 15 Hz

Note: HAWA, E07A, E08A, F07A reflect Saddle Mountain basalt analogs while D08A and E09A are Wanapum basalt analogs.

Table 5 Parameter Variations	
Parameter Variations	Change in Median kappa (κ(s))
Q_o/1.5	κ/1.1
Q_o * 1.5	κ * 1.1
η/1.5	κ/1.4
η * 1.5	κ * 1.1
R_C/1.5	κ * 1.01
R_C * 1.5	κ * 1.004
κ/2	κ * 1.09
κ * 2	κ * 1.004
Δσ * 2	κ * 1.01
Δσ/2	κ/1.004
amp/1.3[1]	κ * 1.05

[1]Replaced Hanford Crustal amplification (Figure 1) with unity. Note relative difference for individual sites varied up to about 10%.

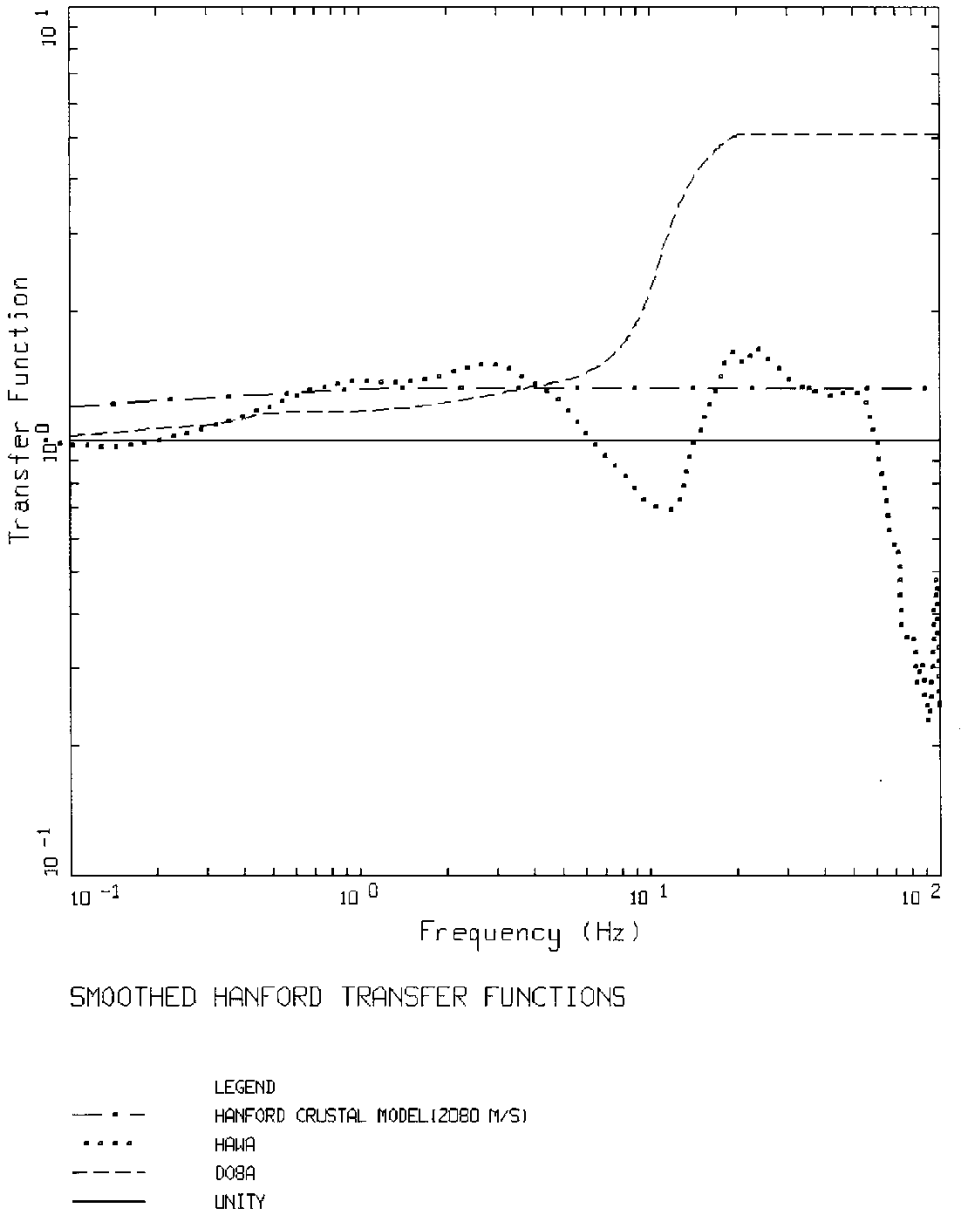

Figure 1. Smoothed Hanford crustal transfer functions for: 1) local crustal model with a surface shear-wave velocity of 2,080m/s, 2) recording site HAWA, 3) recording site D08A.

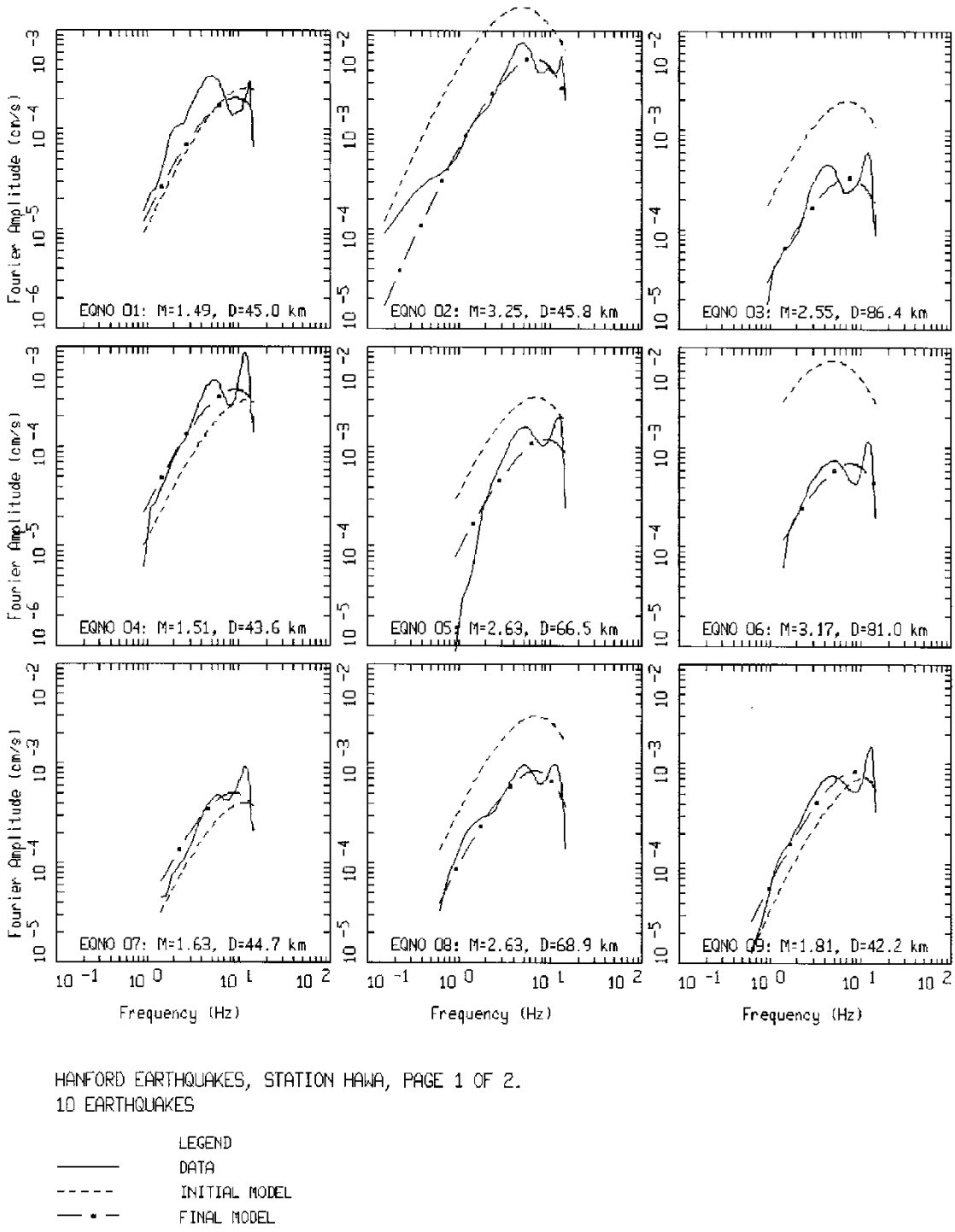

Figure 2. Comparison of model (initial and final) and recording (Table 2) FAS at SMB site HAWA for the ten earthquakes of the 2004 kappa analysis (PNNL, 2005). Logarithmic followed by linear frequency axes.

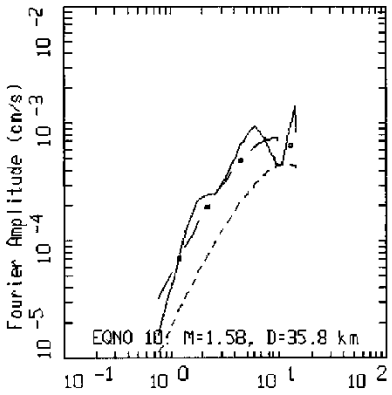

HANFORD EARTHQUAKES, STATION HAWA, PAGE 2 OF 2.
10 EARTHQUAKES

Figure 2 (cont.)

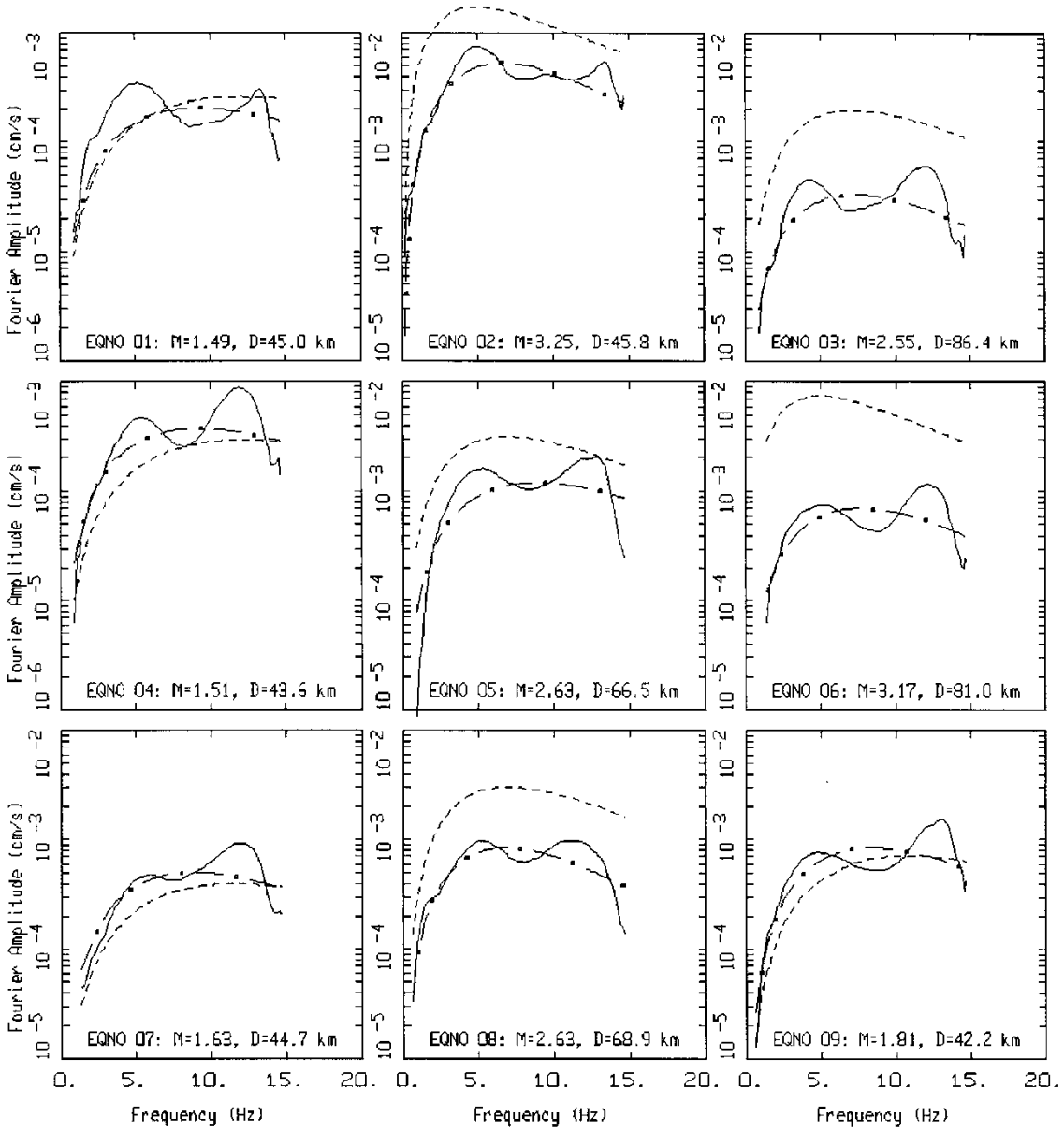

HANFORD EARTHQUAKES, STATION HAWA, PAGE 1 OF 2.
10 EARTHQUAKES

LEGEND
——— DATA
- - - - - INITIAL MODEL
—— • —— FINAL MODEL

Figure 2 (cont.)

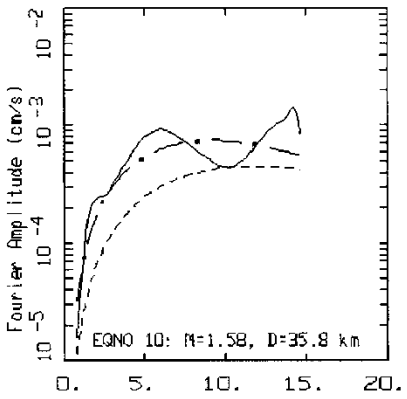

HANFORD EARTHQUAKES, STATION HAWA, PAGE 2 OF 2.
10 EARTHQUAKES

Figure 2 (cont.)

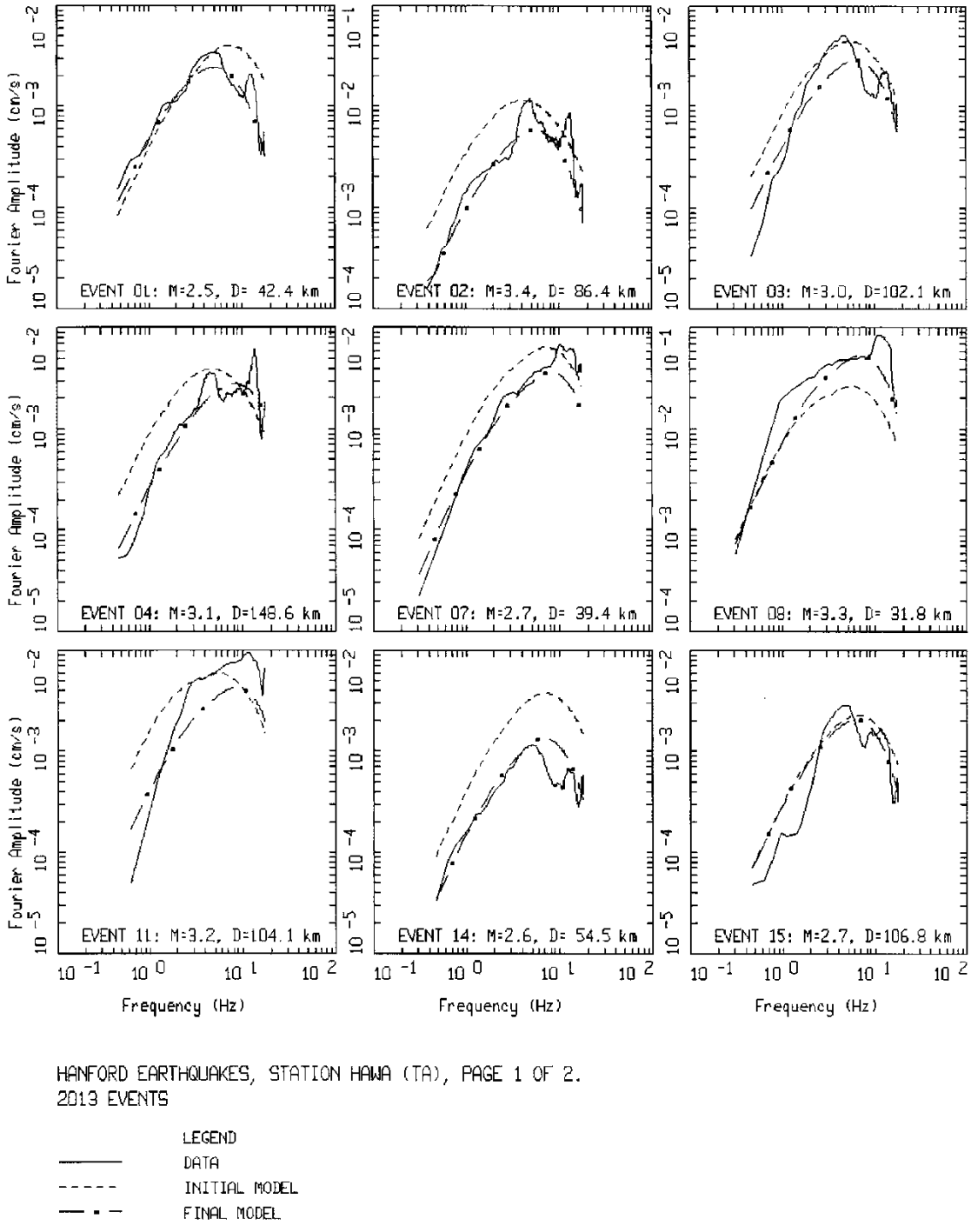

Figure 3. Comparison of model (initial and final) and recording FAS at SMB site HAWA for the fifteen selected earthquakes recorded at the TA array station (Table 3). Logarithmic followed by linear frequency axes.

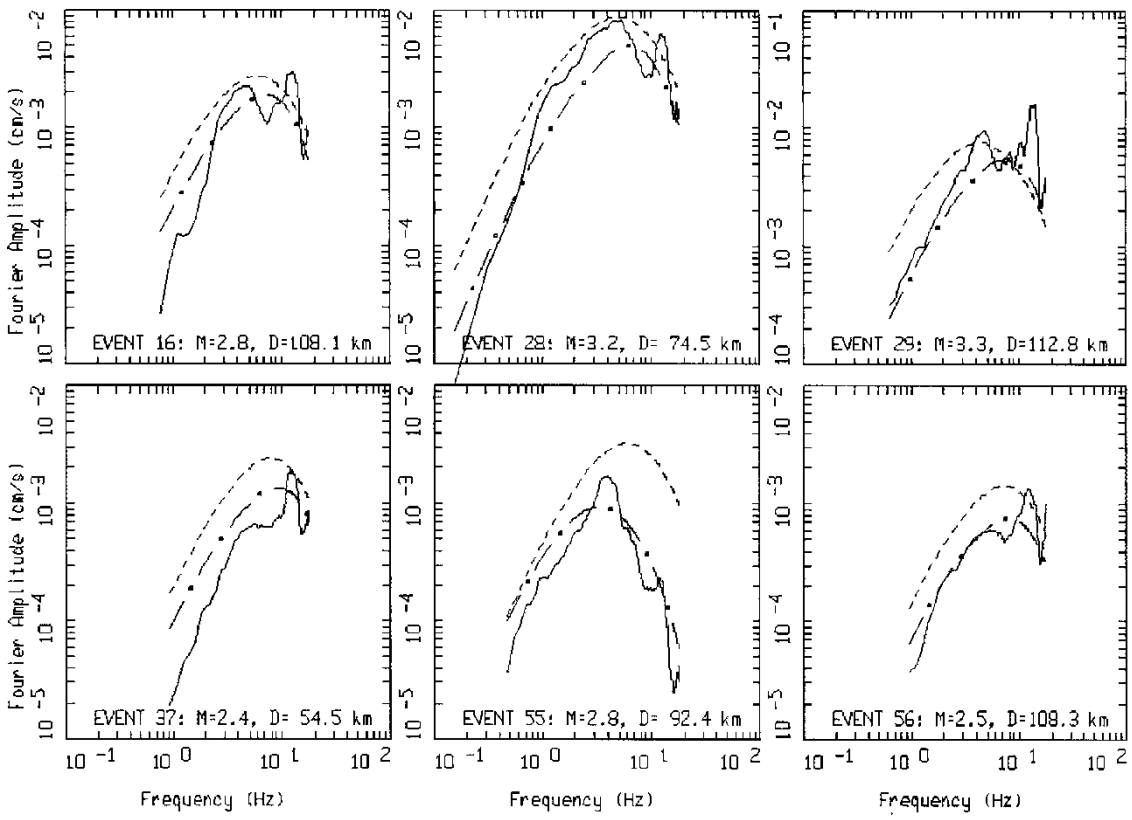

Figure 3 (cont.)

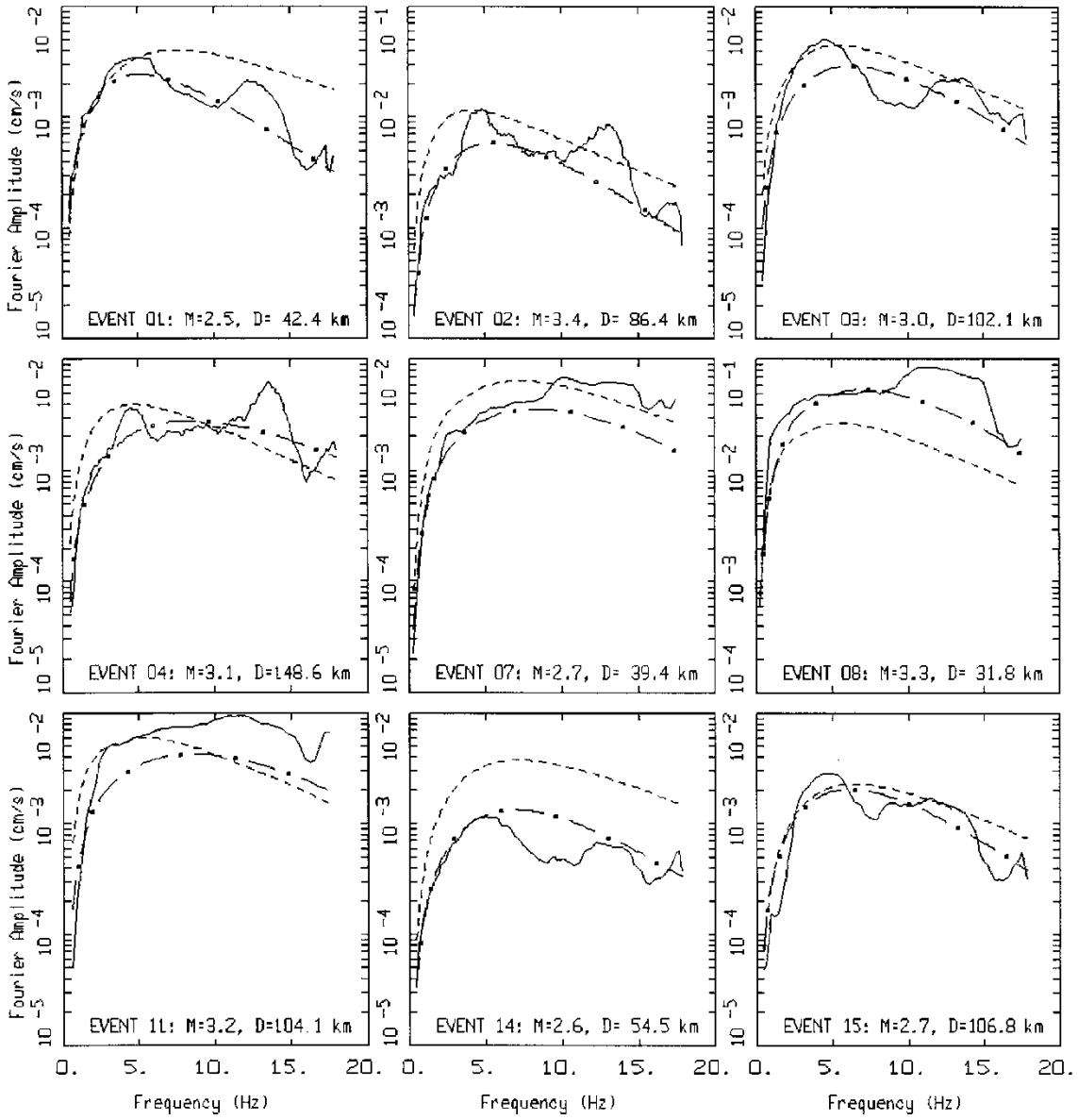

Figure 3 (cont.)

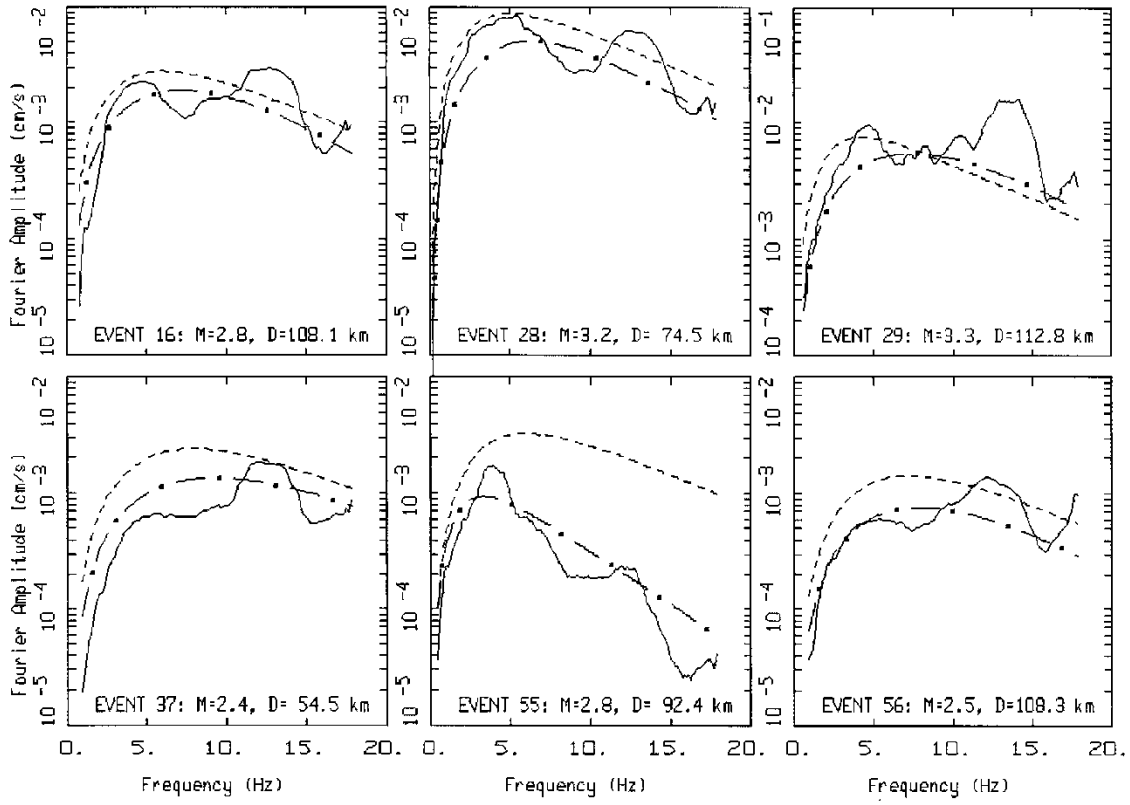

Figure 3 (cont.)

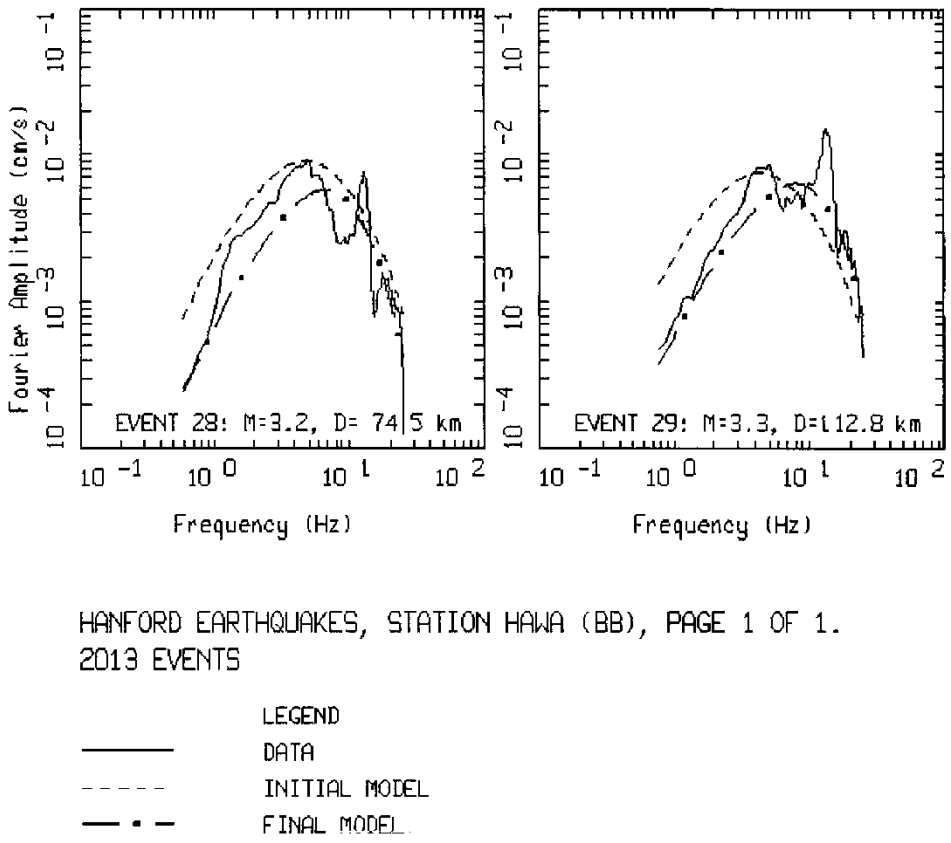

Figure 4. Comparison of model (initial and final) and recording FAS at SMB site HAWA for the two selected earthquakes recorded at the accelerograph station (Table 3). Logarithmic followed by linear frequency axes.

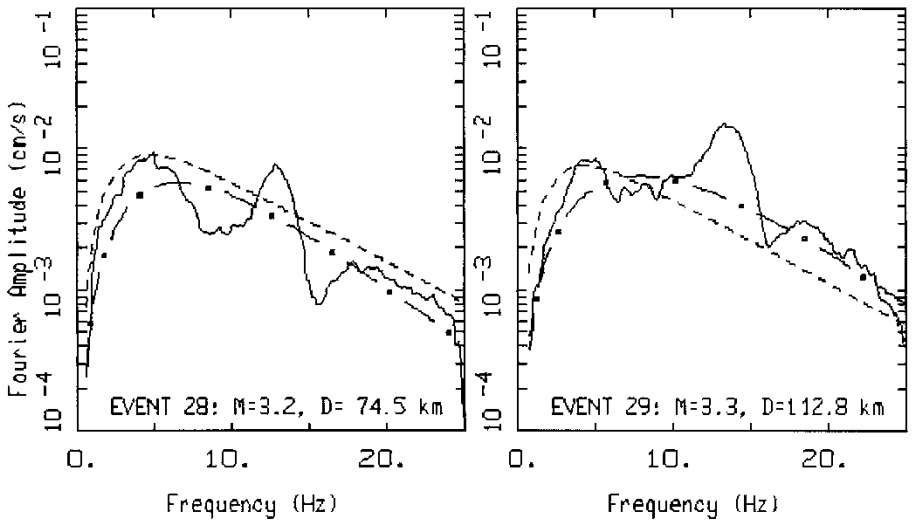

HANFORD EARTHQUAKES, STATION HAWA (BB), PAGE 1 OF 1.
2013 EVENTS

LEGEND
DATA
INITIAL MODEL
FINAL MODEL

Figure 4 (cont.)

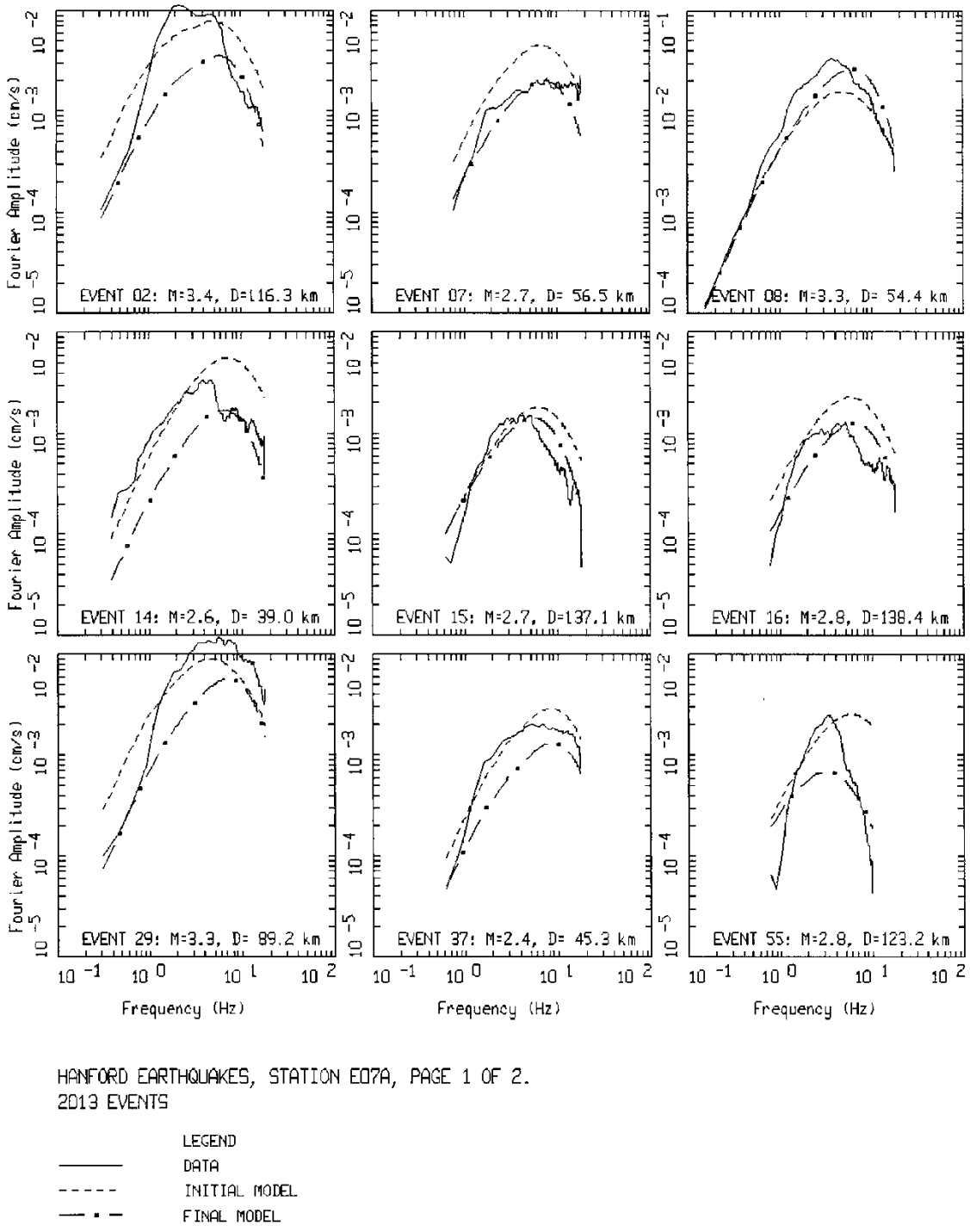

Figure 5. Comparison of model (initial and final) and recording FAS at SMB site E07A for the subset of fifteen selected earthquakes recorded at the TA array station (Table 3). Logarithmic followed by linear frequency axes.

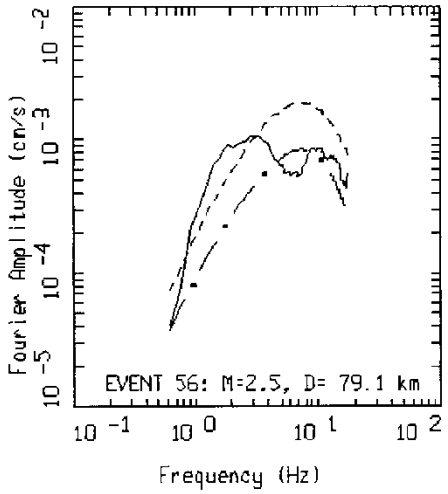

HANFORD EARTHQUAKES, STATION EO7A, PAGE 2 OF 2.
2013 EVENTS

Figure 5 (cont.)

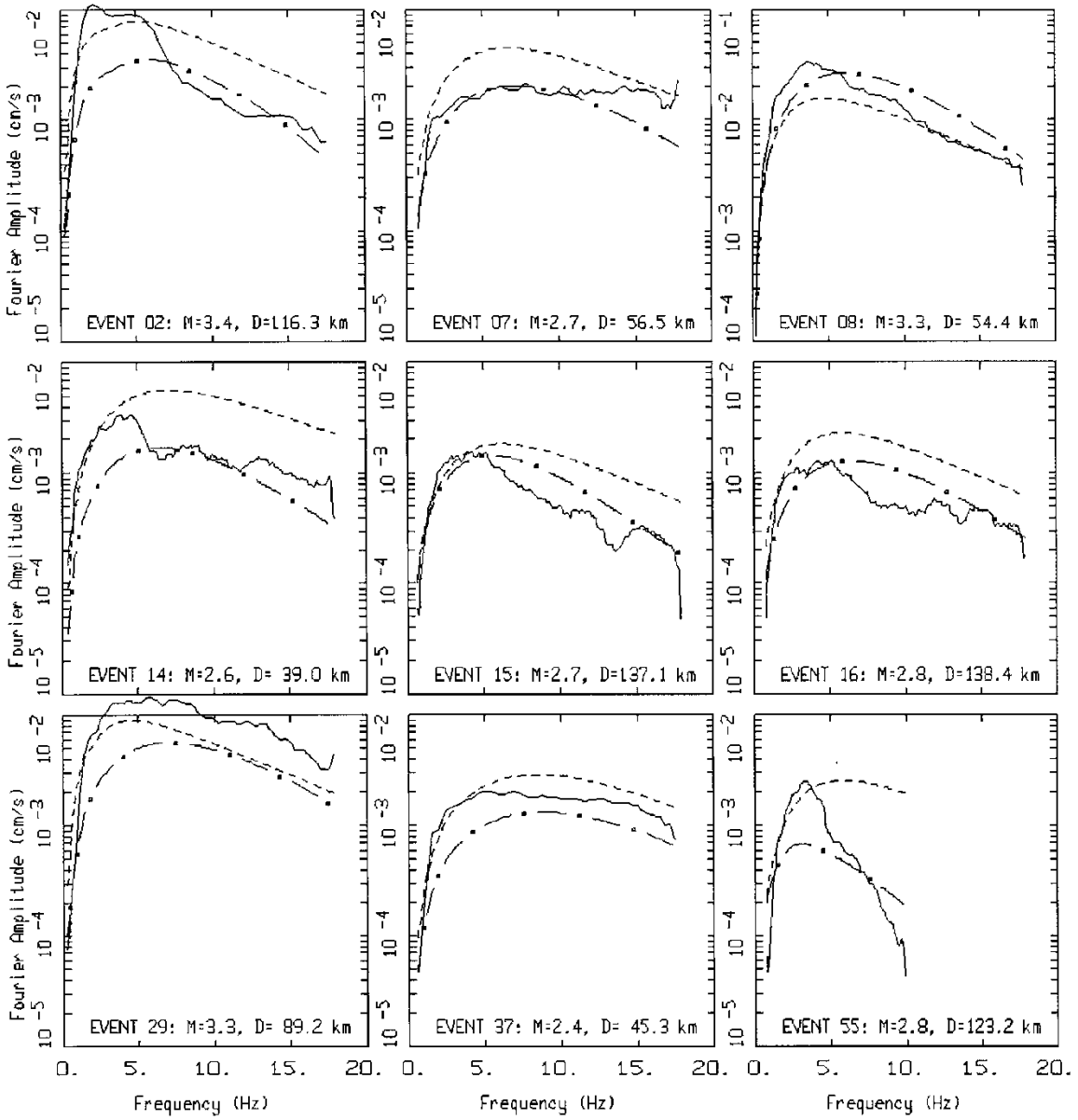

HANFORD EARTHQUAKES, STATION E07A, PAGE 1 OF 2.
2013 EVENTS

LEGEND
——— DATA
- - - - - INITIAL MODEL
—•— FINAL MODEL

Figure 5 (cont.)

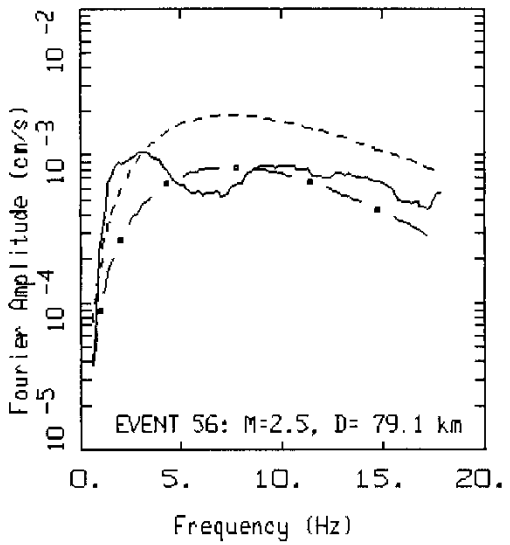

HANFORD EARTHQUAKES, STATION E07A, PAGE 2 OF 2.
2013 EVENTS

Figure 5 (cont.)

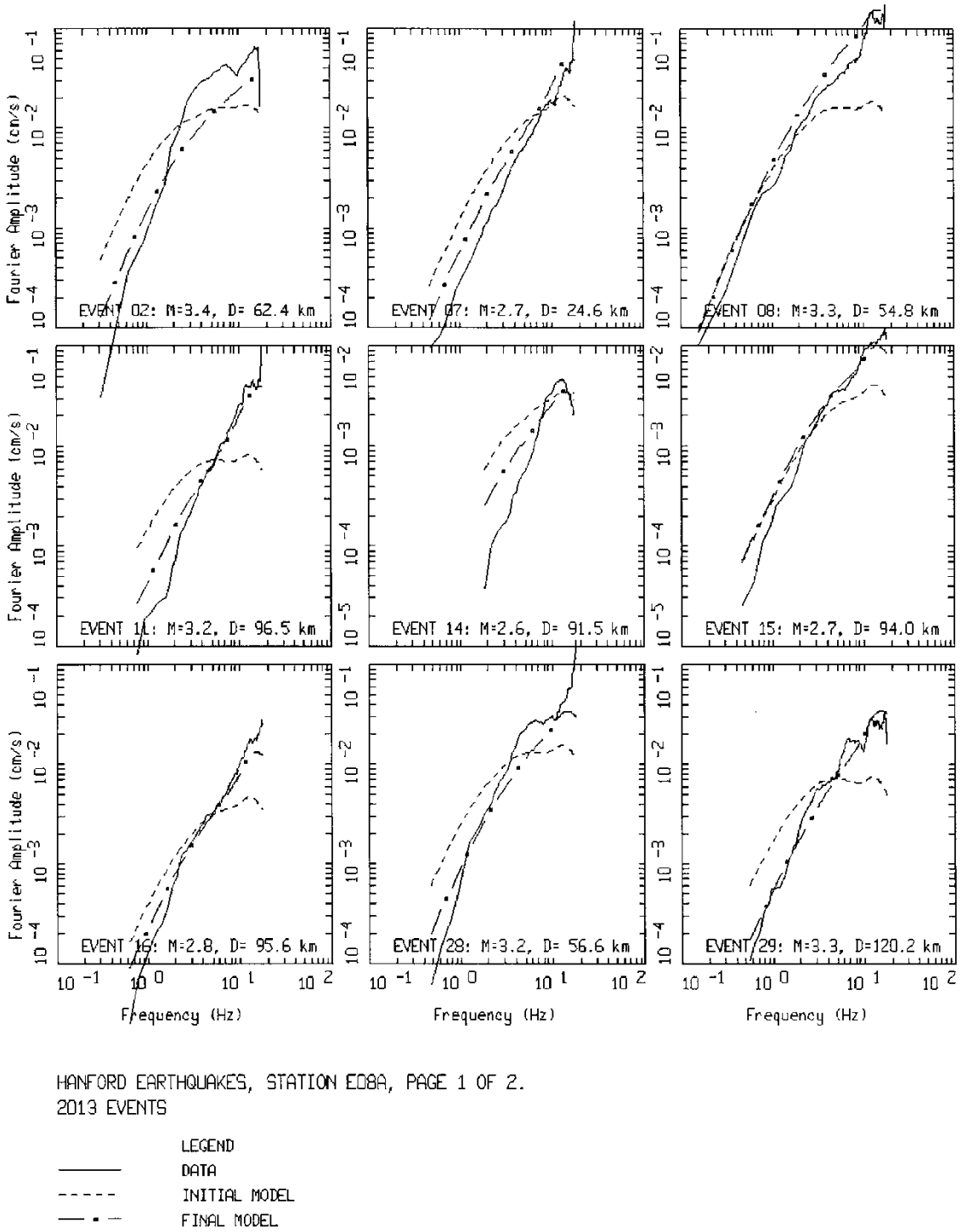

Figure 6. Comparison of model (initial and final) and recording FAS at SMB site E08A for the subset of fifteen selected earthquakes recorded at the TA array station (Table 3). Logarithmic followed by linear frequency axes.

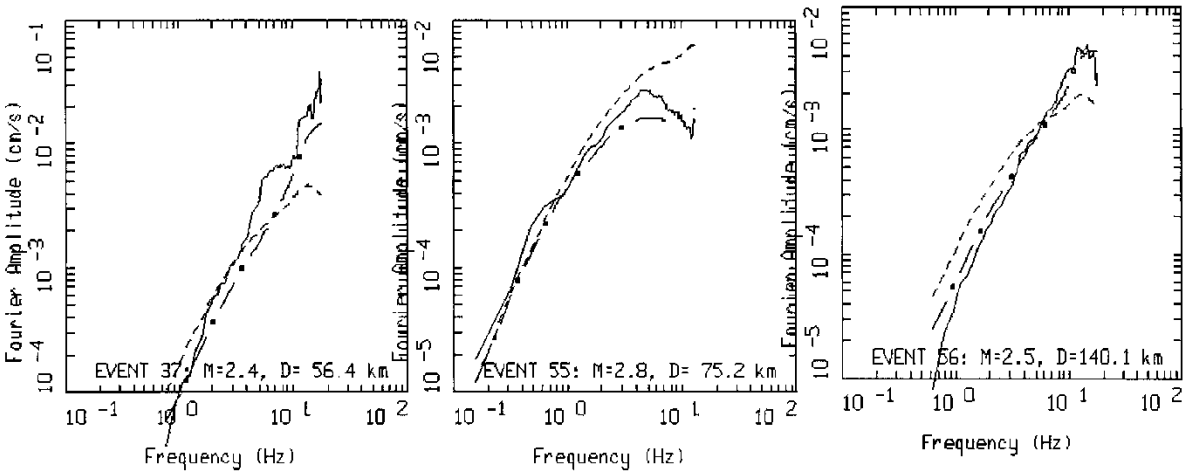

HANFORD EARTHQUAKES, STATION EOBA, PAGE 2 OF 2.
2013 EVENTS

Figure 6 (cont.)

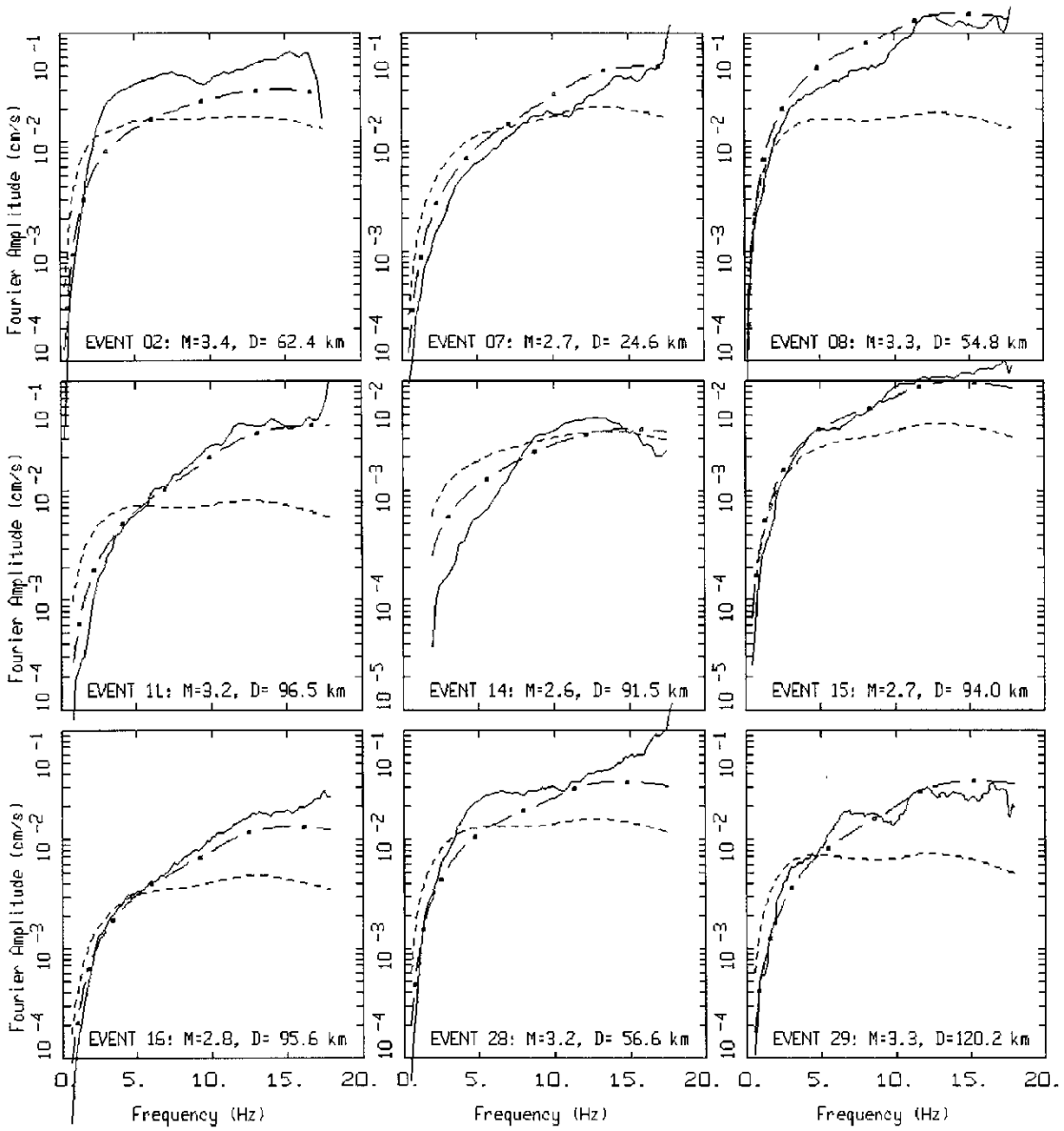

Figure 6 (cont.)

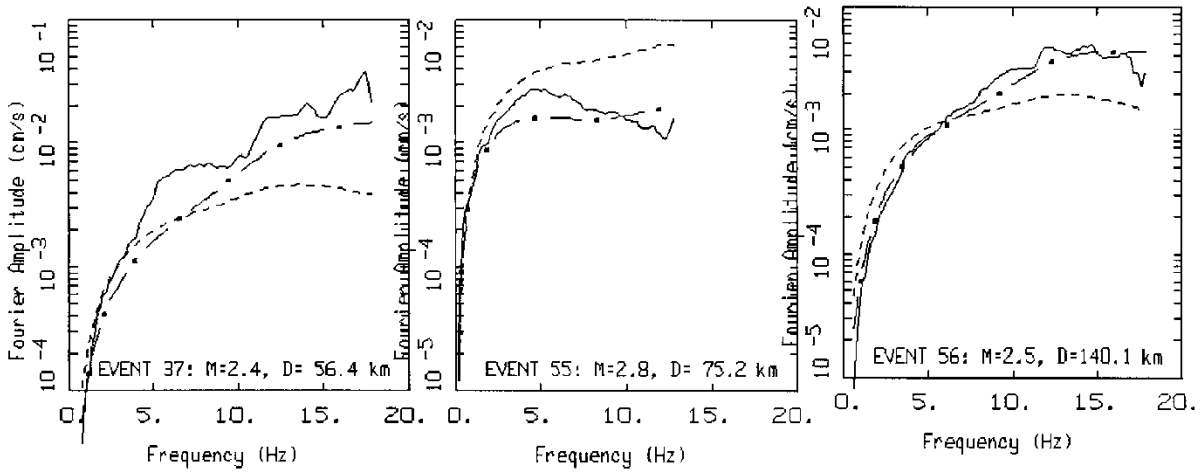

HANFORD EARTHQUAKES, STATION EOBA, PAGE 2 OF 2.
2013 EVENTS

Figure 6 (cont.)

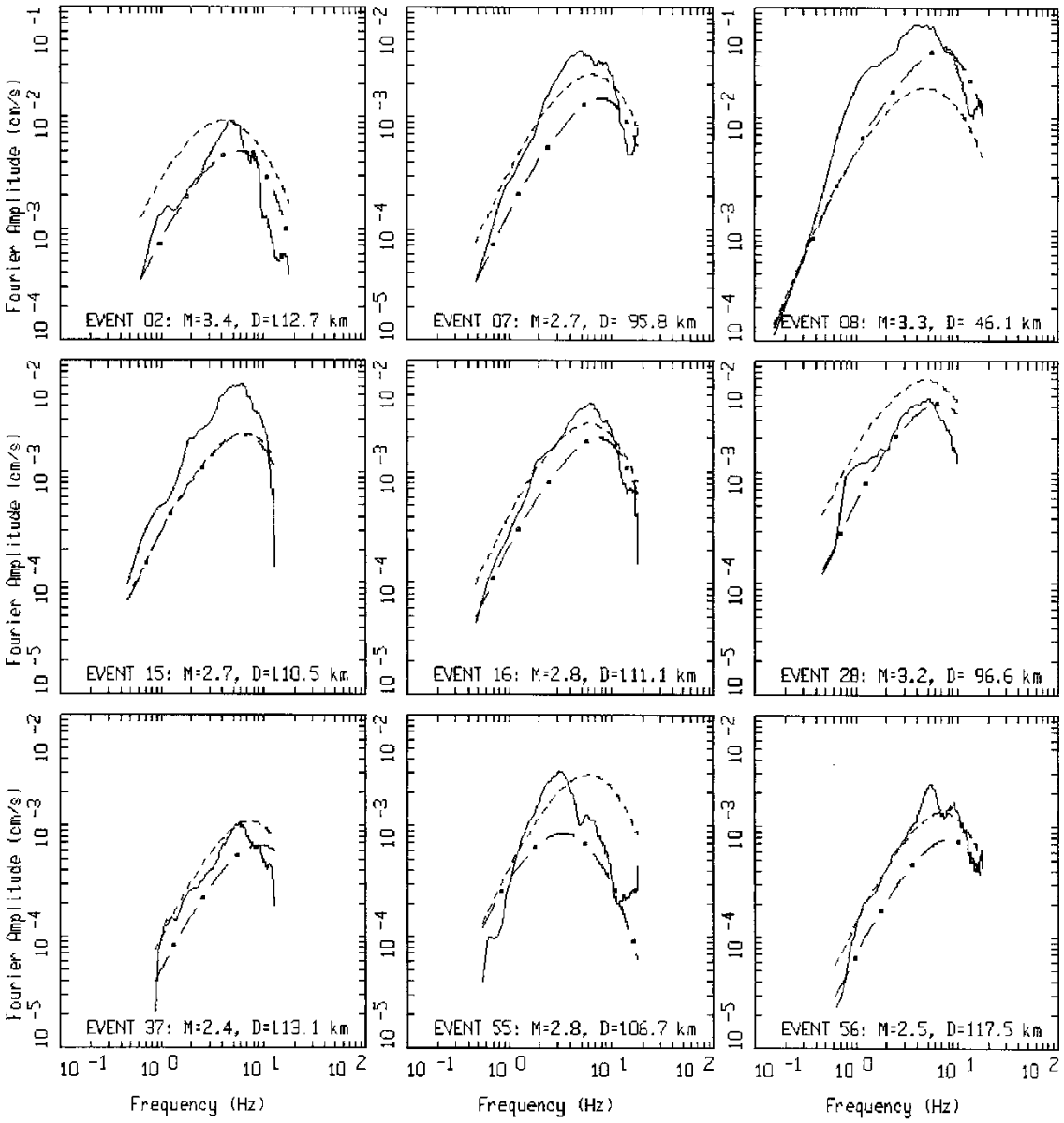

Figure 7. Comparison of model (initial and final) and recording FAS at SMB site F07A for the subset of fifteen selected earthquakes recorded at the TA array station (Table 3). Logarithmic followed by linear frequency axes.

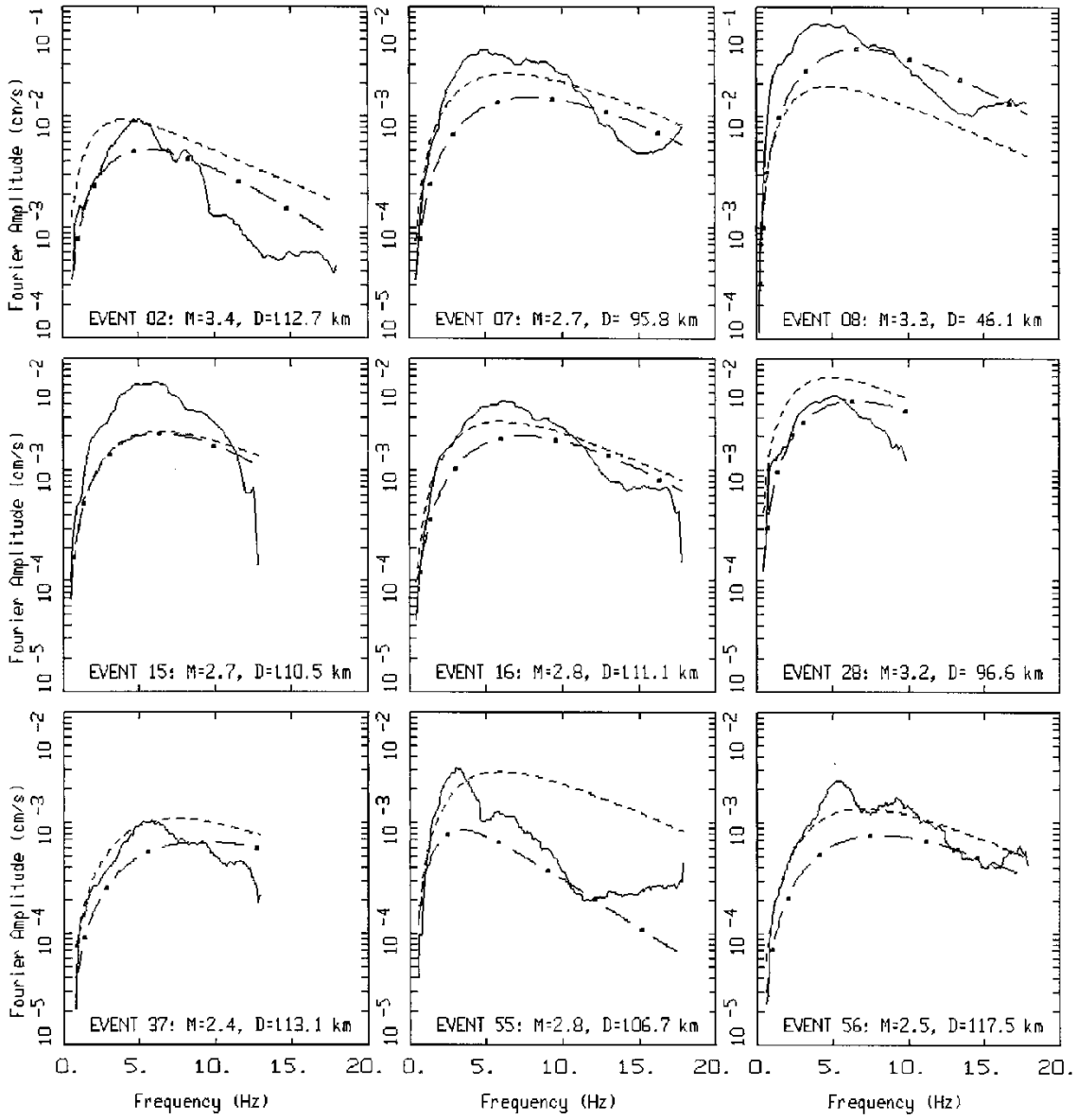

HANFORD EARTHQUAKES, STATION FO7A, PAGE 1 OF 1.
2013 EVENTS

LEGEND
DATA
INITIAL MODEL
FINAL MODEL

Figure 7 (cont.)

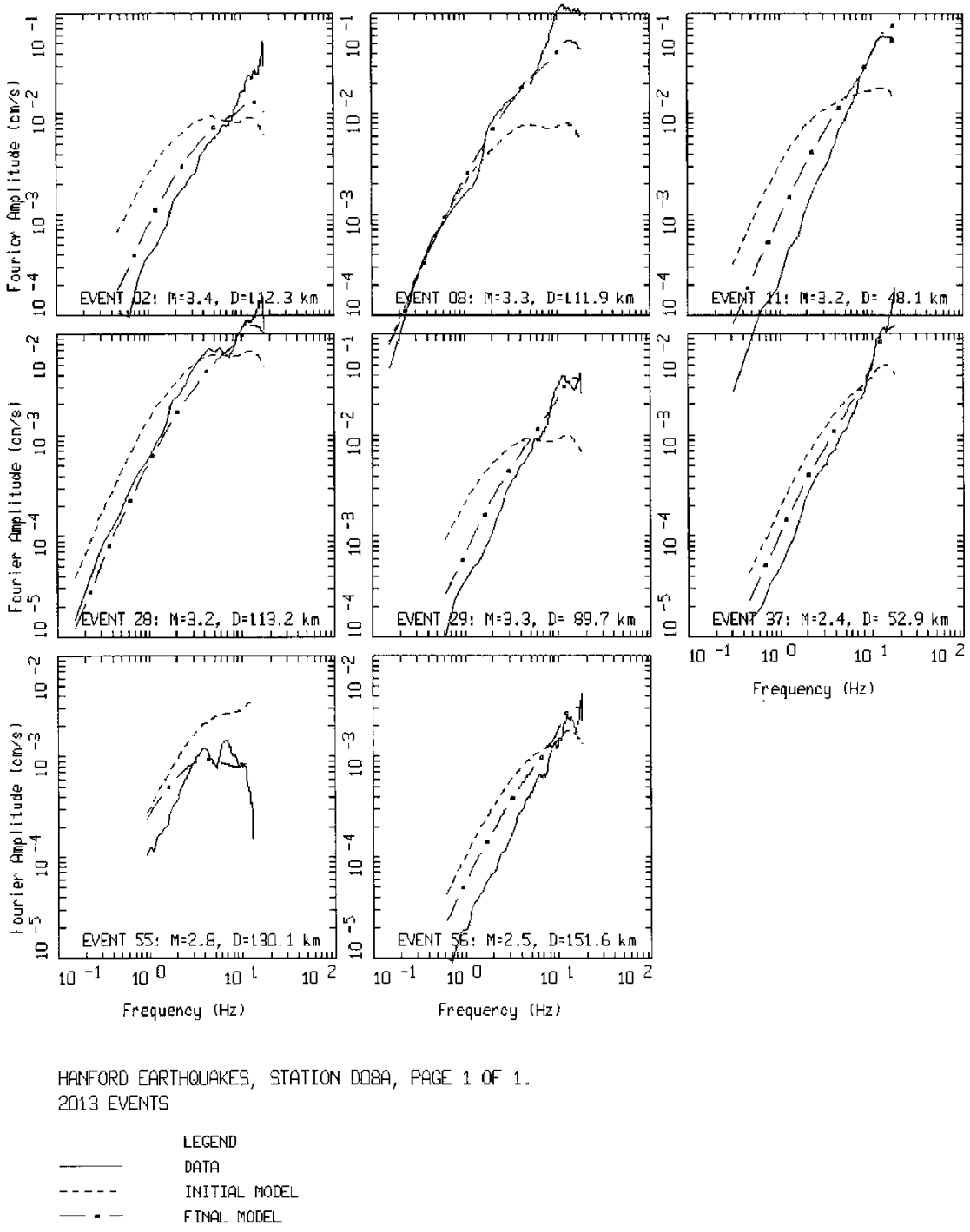

Figure 8. Comparison of model (initial and final) and recording FAS at WB site D08A for the subset of fifteen selected earthquakes recorded at the TA array station (Table 3). Logarithmic followed by linear frequency axes.

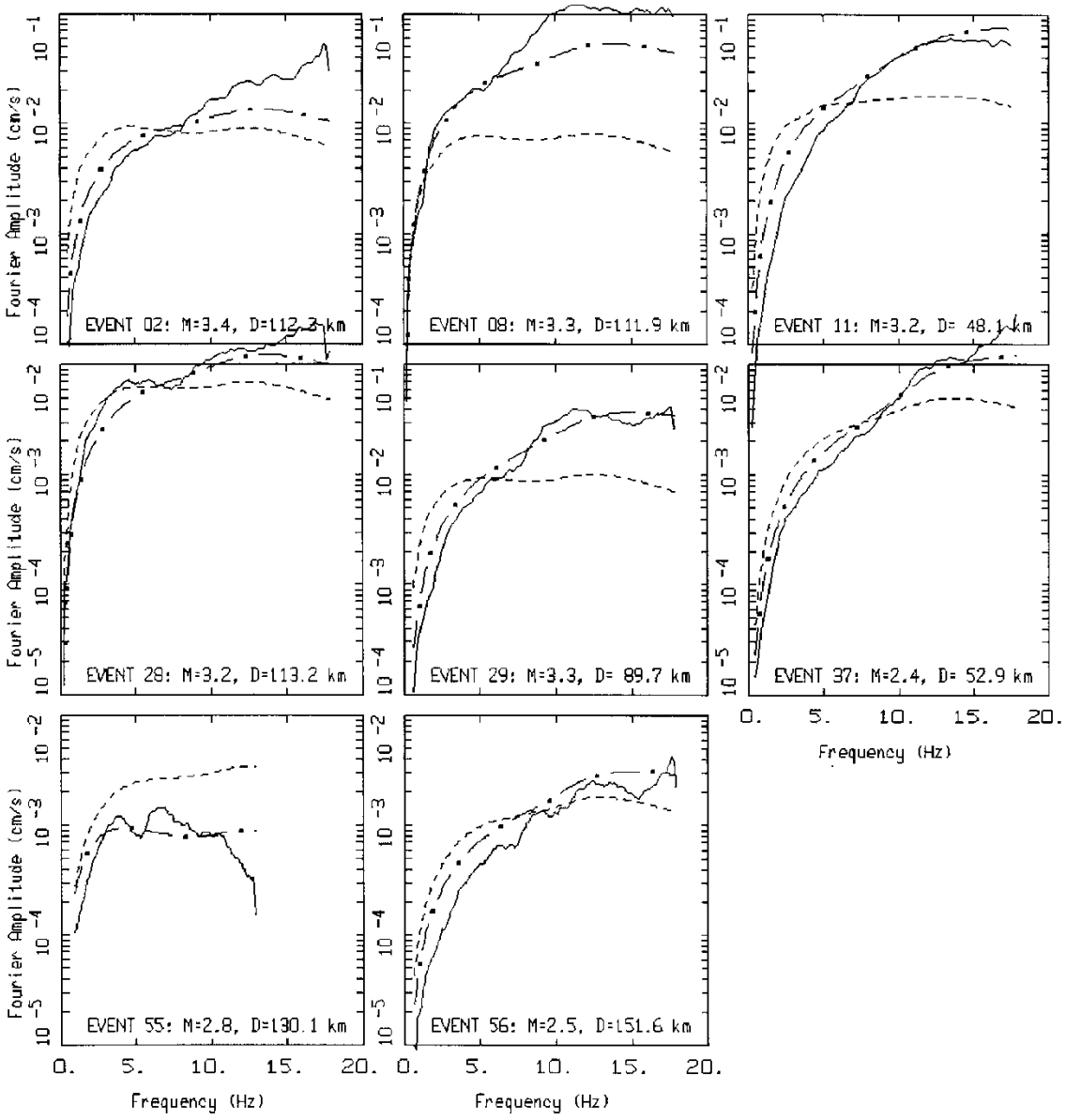

Figure 8 (cont.)

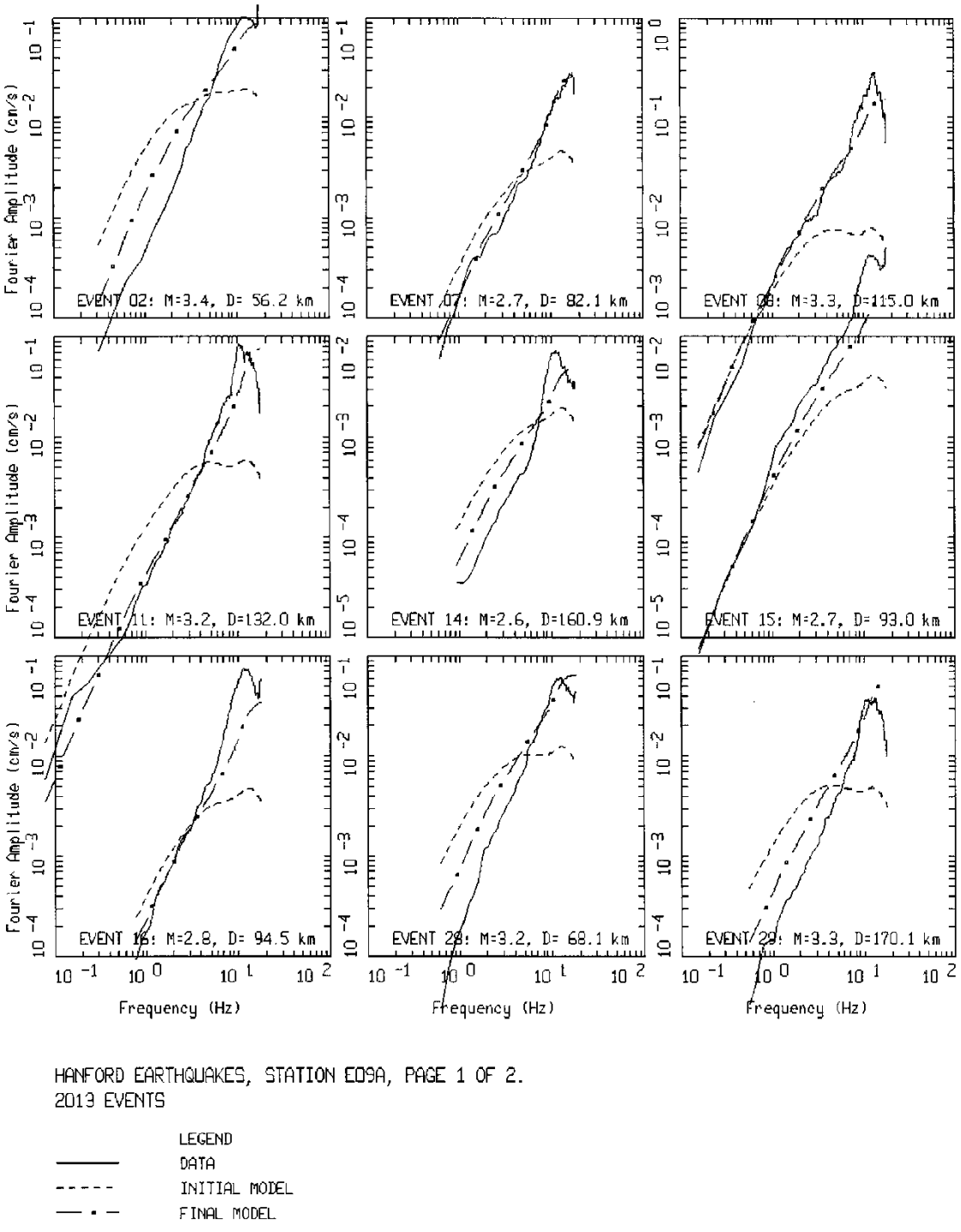

Figure 9. Comparison of model (initial and final) and recording FAS at WB site E09A for the subset of fifteen selected earthquakes recorded at the TA array station (Table 3). Logarithmic followed by linear frequency axes.

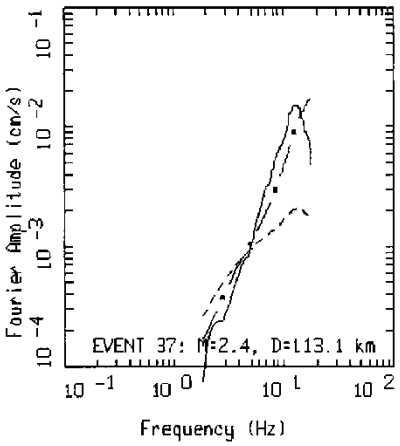

HANFORD EARTHQUAKES, STATION ED9A, PAGE 2 OF 2.
2013 EVENTS

Figure 9 (cont.)

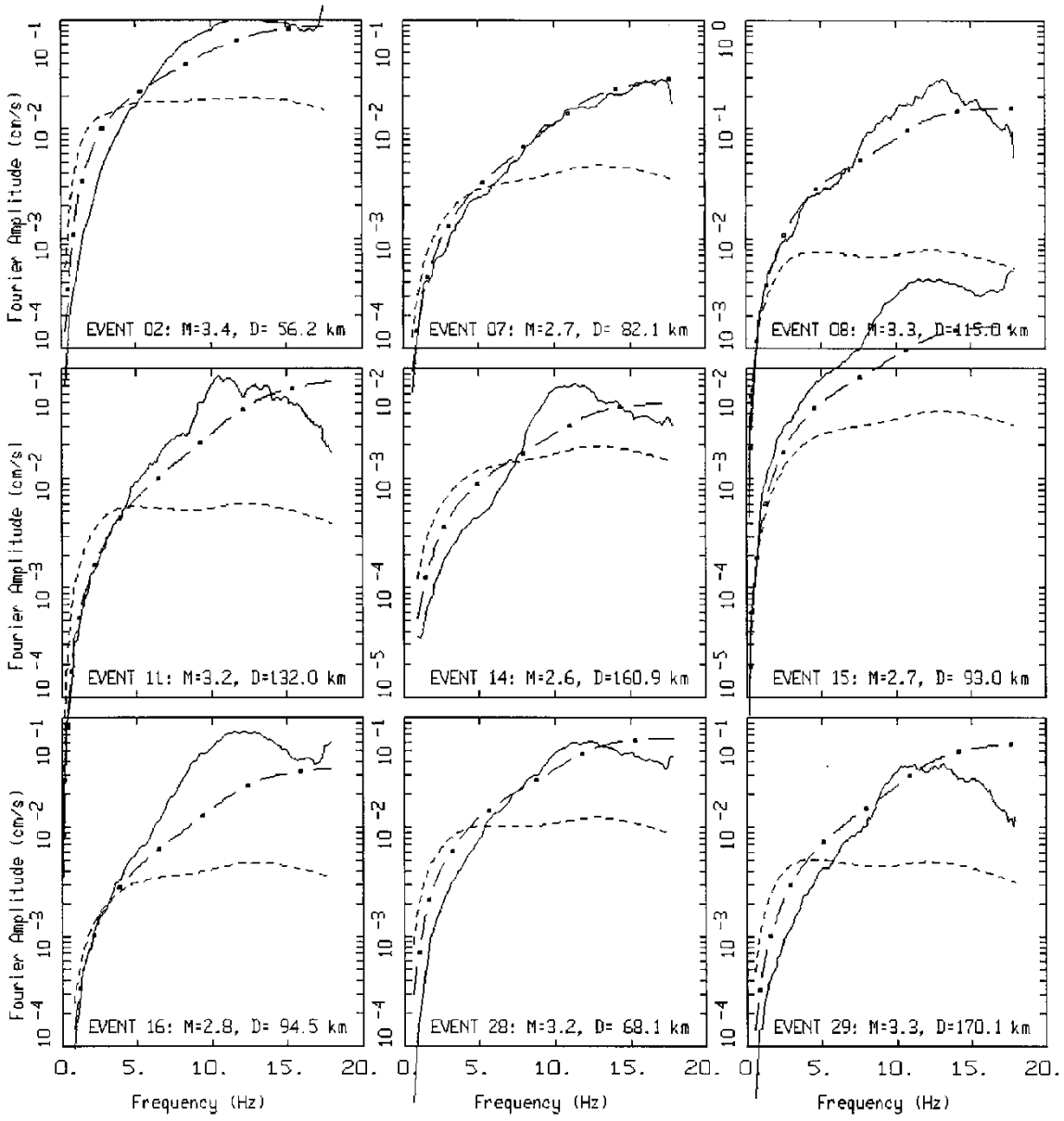

HANFORD EARTHQUAKES, STATION E09A, PAGE 1 OF 2.
2013 EVENTS

LEGEND
DATA
INITIAL MODEL
FINAL MODEL

Figure 9 (cont.)

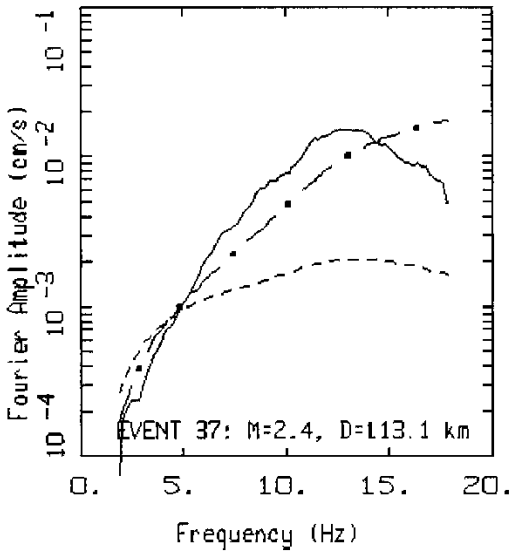

HANFORD EARTHQUAKES, STATION EO9A, PAGE 2 OF 2.
2013 EVENTS

Figure 9 (cont.)